IEEE Robotics and Automation Letters (RA-L) paper, presented at ICRA 2026, Vienna, Austria. Cite as RA-L paper.

A Proximity-Based Framework for Human-Robot Seamless Close Interactions

Liana Bertoni, Lorenzo Baccelliere, Luca Muratore, and Nikos G. Tsagarakis

***Abstract*—The administration and monitoring of shared workspaces are crucial for seamlessly integrating robots to operate in close interactions with humans. Adaptive, versatile, and reliable robot movements are key to achieving effective and successful human-robot synergy. In situations involving unexpected or unintended collisions, robots must react appropriately to minimize risks to humans while still staying focused on their primary tasks or safely resuming them. Although collision detection and identification algorithms are well-established, more advanced robot reactions beyond basic stop-and-wait reactions have not yet been widely adopted and understood. This limitation highlights the need for more sophisticated robot responses to better handle complex collision scenarios, ensuring both safety and task continuity. This letter introduces a novel complete robotic system that leverages the potential of on-board proximity sensor equipment to seamlessly furnish compatible robot reactions while operating in close interactions. With on-board distributed proximity sensors, the robot gains a continuous close workspace awareness, facilitating a transparent negotiation of potential collisions while executing tasks. The proposed system and framework are validated in a collaborative industrial task scenario composed of sub-tasks allocated to the human and the robot and performed within shared regions of the workspace, demonstrating the efficacy of the approach.**

***Index Terms*—Human-robot collaboration, close interactions, proximity sensors, and control framework.**

I. INTRODUCTION

HUMAN-ROBOT seamless close interactions significantly ameliorate tasks execution [1]. Leveraging their complementary strengths, robots can take over heavy and repetitive operations, while humans execute decision-making, domain expertise, and contextual awareness. This collaboration not only reduces human fatigue and cognitive load but enhances overall task performance and reliability [2].

To capitalize on the potential of human-robot teamwork, fluent and dynamic interactions between the two parts should be achieved [3]. Trustworthy [4], coefficient [5], or timely robot responses [6] have been shown to elicit human-perceived natural behavior in robot motion, contributing to smoother and intuitive interactions. Moreover, coordinated and synchronized robot movements permit reducing task execution time, thereby enhancing the efficiency and productivity of shared tasks [7], [8]. [9] emphasizes that while fundamental collision avoidance strategies are well-established, there remains a critical gap in the development of more refined, context-aware reactive behaviors that allow robots to adapt intelligently during close interactions.

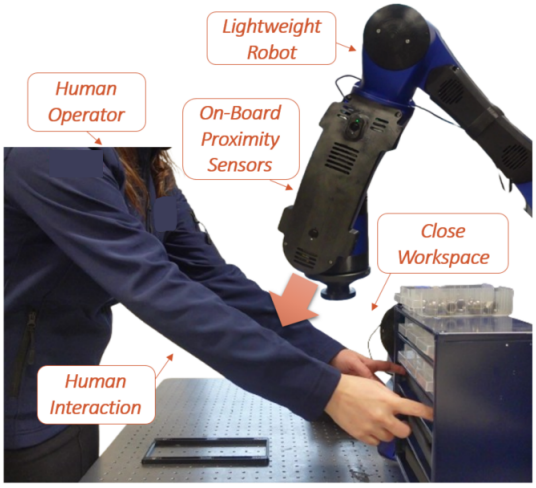

Fig. 1. *Human-Robot Seamless Close Interactions: human and a robot work on a shared task while synergistically covering different task operations.*

This letter presents a novel robotic system that leverages the on-board proximity sensors to enhance seamless human-robot close interactions. This system features a custom lightweight robotic arm integrated with an on-board proximity sensing arrangement on the forearm, combined with a control framework. Enabling a continuous and precise awareness of the robot's close workspace, the robot can dynamically adjust its movements in response to the human's position, ensuring safety and efficiency. These capabilities result in smoother and more natural interactions, optimizing the effectiveness of shared task execution. The developed algorithms utilize the provided distance measurements to appropriately guide robot movements and reactions when working closely with humans during shared task execution. Specifically, the developed robot planning and control framework allows for adaptation to unintended contacts through localized motion re-planning and modulation strategies for robot impedance, further enabling compliant behaviors during close interactions and collision avoidance. The overall system provides (i) continuity of the robot operations during interactions, (ii) fast computations, and (iii) robot reactions in a short range of distance.

The proposed robotic system has been experimentally

Manuscript received: January, 17, 2025; Revised: April 21, 2025; Accepted: June 13, 2025. This paper was recommended for publication by Editor Gentiane Venture, upon evaluation of the Associate Editor and Reviewers' comments.

Liana Bertoni is with the Humanoids and Human-Centered Mechatronics (HHCM) Lab, Istituto Italiano di Tecnologia (IIT), 16163 Genova, Italy, and also with the Department of Information Engineering (DII), University of Pisa, 56126 Pisa, Italy.

Lorenzo Baccelliere, Luca Muratore, and Nikos G. Tsagarakis are with the Humanoids and Human-Centered Mechatronics (HHCM) Lab, Istituto Italiano di Tecnologia (IIT), 16163 Genova, Italy. Authors contacts are available at {liana.bertoni (corresponding author), lorenzo.baccelliere, luca.muratore, nikos.tsagarakis}@iit.it

This work was supported by the HARIA project (EU Horizon Europe, GA No. 101070292).

Digital Object Identifier (DOI): see top of this page.

IEEE Robotics and Automation Letters (RA-L) paper, presented at ICRA 2026, Vienna, Austria. Cite as RA-L paper.

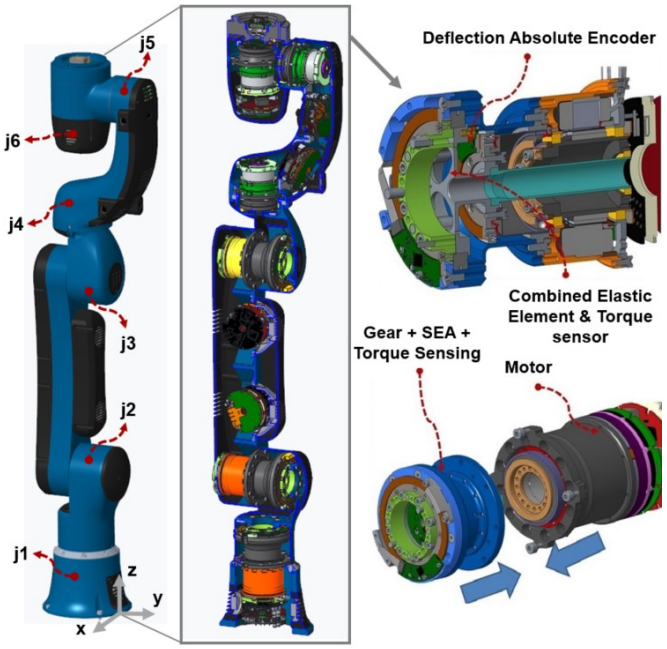

Fig. 2. *Structural and Actuator Design of the Custom Lightweight Robotic Arm*. On the left, the complete exterior of the arm and the internal configuration are shown, highlighting the arrangement of actuators within each joint. A detailed view of a single actuator module is provided on the right.

demonstrated during the execution of i) a co-assembly task and ii) an assisted assembly task. Section II provides the related works, Section III gives a robotic arm description, and the proposed framework is described in Section III. Sections IV and V conclude the work with the experiments and conclusions, respectively.

II. RELATED WORKS

Initial safety frameworks, which handled the human shared workspace have primarily been developed to meet ISO standard requirements [10]. While these frameworks have undoubtedly improved safety, they tend to be overly cautious, emphasizing protection over performance. Consequently, in collaborative settings, where human-robot interaction is essential, such frameworks can lead to reduced efficiency, as they impose slowdowns or even complete halts in robot operations when safety boundaries are exceeded. Although beneficial in traditional scenarios, this strict adherence to safety guidelines is not always suitable for dynamic, interactive, and real-time human-robot collaboration. As a result, the need for more flexible, context-aware safety mechanisms has become increasingly apparent. In this direction, over predefined paths, [11] proposes an improved velocity scaling using the braking surface method that enables faster robot operation near humans. Instead, attempting to improve existing optimization problems regarding cost computation time in planning safe trajectories, the work in [12] introduces an optimization problem with a search-based approach. By employing a well-informed graph, the method produces robot trajectories to avoid static obstacles. Meanwhile, [13] presents an energy-based trajectory optimization to produce faster robot motion, exploiting an inertia scaling to avoid static obstacles. [14] combines multiple safety layers to enhance robot responsiveness in more dynamic environments. However, despite efforts to move beyond conventional pre-collision safety schemes, these solutions remain limited in scope. The methods are predominantly validated in static or highly controlled environments, falling short of the demands and unpredictability of real-world collaborative scenarios. This gap limits their applicability to dynamic, shared workspaces where continuous adaptation and responsiveness are essential. Moreover, most of these approaches rely on camera-based systems for detecting humans or obstacles. Such systems are inherently constrained by occlusions and dependency on line-of-sight, which restricts their reliability and effectiveness in cluttered or fast-changing environments.

Free from occlusions, on-board proximity sensors [15] provide a compelling solution to unlock robot seamless close interactions with humans. Works, such as [16]–[18], employ on-board capacity-based proximity sensors to avoid dynamic collisions. [19] uses a vision-proximity based system to position the robot in a cluttered space. In [20], proximity sensors are used to elude collisions while following a path, and in [21], collisions with humans are tackled by stopping the robot motion. Unlike previous studies that primarily focus on collision avoidance, our work integrates proximity sensors to facilitate seamless human-robot close interactions aimed at efficient shared task execution. Furthermore, in contrast to capacitive or inductive sensor-based approaches, which often require complex calibration procedures and are sensitive to material properties that can affect measurement accuracy, we utilize Time-of-Flight (ToF) sensors. These sensors offer a more straightforward and efficient method for obtaining distance measurements, thereby enhancing overall system reliability. Lastly, in contrast to [22], where the close workspace of the robot is continuously analyzed and divided into portions where the robot is allowed or not to operate, our work offers a reaction-oriented solution fostering operations continuity.

TABLE I
SPECIFICATIONS OF THE ACTUATORS

Type	Gear ratio	Joint num.	Maximum velocity	Torque(Nm) peak-cont.	Power(W) peak-cont	Torque res.	Mass (Kg)
MA	160	1,2	5.7 rad/s	147-90.4	837-480	11 bits	1.32
MB	160	3	8.2 rad/s	147-52.9	1286-432	11 bits	1.15
S	100	7	20.3 rad/s	27-9.2	556-171	10 bits	0.74

TABLE II
SPECIFICATIONS FOR THE RANGE OF MOTION

Joint Num.	Joint Type	Range of Motion
j1	Shoulder Yaw	+160, -160
j2	Shoulder Pitch	+120, -120
j3	Elbow Pitch	+130, -130
j4	Forearm Yaw	+160, -160
j5	Wrist Pitch	+135, -135
j6	Wrist Yaw	+155, -155

III. ROBOTIC ARM DESCRIPTION

In this Section, the custom lightweight robotic arm integrated with onboard proximity sensors is detailed. As depicted in Fig. 2, the prototype arm exhibits a compact and streamlined mechanical structure. The design prioritizes low inertia, high back-drivability, and integrated sensing to meet the demands

IEEE Robotics and Automation Letters (RA-L) paper, presented at ICRA 2026, Vienna, Austria. Cite as RA-L paper.

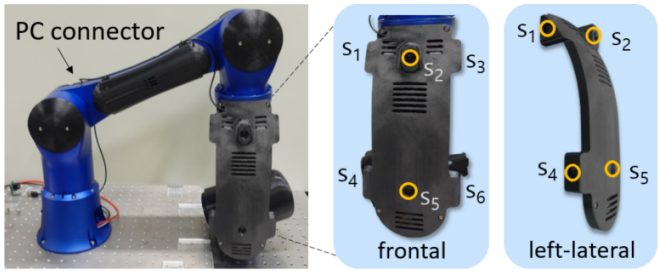

Fig. 3. *On-Board Proximity Sensors Arrangement.* The 6DOF custom lightweight robotic arm integrates ToF-based proximity sensing on its forearm as shown in the picture.

of physical human–robot interaction. The arm features a 6-degree-of-freedom (DOF) kinematic structure, consisting of a 2-DOF shoulder mechanism for wide-range orientation control, a single-DOF elbow joint for efficient reach and folding, and a 3-DOF wrist complex that offers dexterous end-effector positioning and orientation. The realization of the arm is based on the integration of six Series Elastic Actuator (SEA) units along the kinematic chain. SEA technology serves a dual purpose: it protects the reduction gear from impacts while also enabling precise measurement of actuator torque by monitoring the deflection of the elastic element using high-resolution absolute encoders. The arm design incorporates an exoskeleton structure for the interconnection of actuator units. In this design, the actuators' bodies float within the exoskeleton, while the actuators themselves are fixed to the link structures. This exoskeleton and floating actuation integration approach offers several key advantages. Unlike traditional endoskeleton designs, where actuator bodies bear the load, the floating actuator bodies in this design are not subjected to joint torques or forces. These forces are instead transmitted solely through the two output flanges that secure the actuator to the structure. As a result, the design allows for an optimal, lightweight construction of the actuation housing components, which are shielded from joint loading. This not only enhances the efficiency of the system but also contributes to a more compact and robust design. The cell parts of the link structures were made from Aluminium T6-7075 (Ergal). The same material was used for the housing components of the harmonic gearbox and the interface flanges used to connect the actuation module to the link structures. For the realization of the arm joints, 3 sizes of actuation were developed: Medium A (MA), Medium B (MB), and Small (S). The actuators specification are provided in Table I and their arrangement is shown in Fig. 2. With a total length of 1.02 meters and a mass of approximately 10.5 kilograms, the system maintains a favorable power-to-weight ratio suitable for mobile or collaborative platforms. It is capable of continuously handling payloads up to 4 kilograms without compromising performance or safety. To ensure compliant behavior during physical interactions, the arm employs a torque-controlled actuation scheme. Each joint integrates brushless DC (BLDC) motor units coupled with harmonic drive gear reducers, offering high torque density and smooth transmission. Embedded joint torque sensors enable real-time feedback control, allowing the robot to modulate its dynamic response. The robot arm is equipped with onboard proximity sensing realized by integrating the lower arm section (forearm) with an array of Time of Flight (ToF) sensor units. The ToF sensors have been integrated into the robot's cover (central images), including two sensors in front and two on each of the lateral sides of the forearm section. The incorporation of proximity sensing only in the forearm body section was considered because the lower arm is more likely to be close to human body parts. An arrangement of 6 sensors over the robot's body was sufficient to detect the human arm. The range varies from 0.05m up to 2m with a sensor weight of 20 grams and a size of 28x13.2 mm. The accuracy is about 0.03m with a resolution of 0.001m. The ToF sensors are commercial sensors [23]. Our current prototype features proximity sensors mounted solely on the robot's forearm. This design decision was made to simplify the initial hardware integration and validate our collision avoidance algorithm for the intended use case. To increase robot workspace coverage, more sensors can be transparently integrated on the arm. Importantly, the algorithm processes each sensor reading in a uniform manner (detailed in Section IV). The number or placement of sensors does not affect their correctness or performance. Thus, expanding sensor coverage to the rear or right side would not further impact the algorithm's functionality.

IV. HUMAN-ROBOT SEAMLESS CLOSE INTERACTIONS CONTROL FRAMEWORK

This section introduces the proposed framework, composed of planning and control of the robot leveraging the onboard proximity sensors measurement.

A. Human-Robot Seamless Close Interactions Planner

In a shared task execution with a human operator, the robot is in charge of some operations of a complete task. A list of task operations to be accomplished by the robot constitutes the inputs of the proposed framework. A task operation is described with: (i) operation target, 6D pose in the Cartesian space, $p^o_{ref} \in \mathbb{R}^6$, and (ii) operation requirements, an operation force $w^o_{ref} \in \mathbb{R}^6$ to realize and an operation precision $\Delta x^o_{ref} \in \mathbb{R}^6$ to satisfy. Given these inputs, the operation planner provides the robot trajectory $p^o_{ref}(t)$ to reach the target, considering the robot moving in free-motion space. Meanwhile, the operation requirement planner computes the operation requirement profiles, $\Delta x^o_{ref}(t)$ and $w^o_{ref}(t)$, respectively, that are necessary for the robot's compliance during task execution. The operation requirement profiles are sent to the impedance modulation, which is detailed in III. B. To enable the robot to operate near the human operator transparently, as well as reduce the robot task operations interruptions, the proximity-aware local trajectory re-planning is dedicated to detecting and avoiding possible collisions by online modifying the planned operation trajectory. In particular, being aware of the state of the workspace in the close vicinity of the robot, free from occlusions, the potential contacts or collisions during shared task execution are administered as follows. Given as an input a threshold for the distance, $d_{safe} \in \mathbb{R}$, a potential contact is detected if at least one sensor over n_s available sensors measures a distance $d_{s_i} \in \mathbb{R}$ where $i = 1, ..., n_s$ lower than the threshold: $d^{s_i} < d_{safe}$. The threshold can be set with a static value or vary over time. If the inequality is violated, then the proximity-aware local trajectory re-planning

IEEE Robotics and Automation Letters (RA-L) paper, presented at ICRA 2026, Vienna, Austria. Cite as RA-L paper.

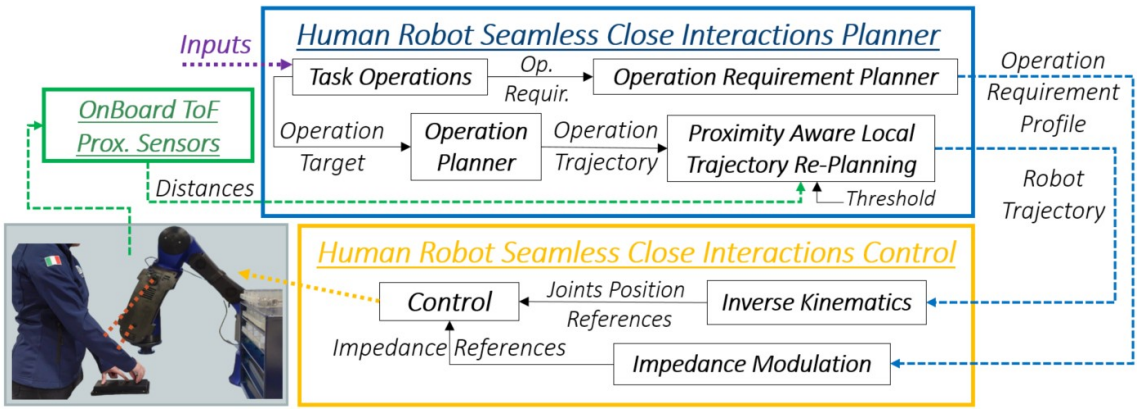

Fig. 4. *Schematic Overview of Human-Robot Seamless Close Interactions Framework.* The framework is composed of three main components: the on-board ToF proximity sensors, the human-robot seamless close interactions planner, and the human-robot seamless close interactions control.

is engaged to compute an online local trajectory re-planning of the operation trajectory. Otherwise, the operation trajectory planned by the operation planner is directly sent to the control layer without any modifications. In the case of modification, we compute

$$p_{ref}(t) = p^o_{ref}(t) + p_c(t), \tag{1}$$

where $p_c(t) \in \mathbb{R}^6$ corrects the planned operation trajectory based on the proximity sensor measurements as

$$p_c(t) = -s(t)\hat{p}_s(t), \tag{2}$$

where $s(t) = \gamma(t)(d_{safe} - d_{s_i}(t)) \in \mathbb{R}$ defines the amount of correction for the operation trajectory. $\hat{p}_s(t) \in \mathbb{R}^6$ is the unit vector providing the direction of the correction, and the negative sign enables the correction of the operation trajectory to generate robot movements in the opposite direction of the detected collision. $\gamma(t) \in \mathbb{R}$ varies from 0 to 1 to generate a smooth trajectory. The amount of correction of the operation trajectory is equal to the difference between the distance threshold and the measured distance. If more sensors retrieve a measured distance less than the defined threshold, $s(t)$ is selected to be the larger value; meanwhile, $\hat{p}_s(t)$ is given by the sum of the sensors that detected the collision. This ensures the computation of the proper direction of the collision avoidance if more sensors detect the collision.

Once the collision is avoided and the safe distance restored, the proximity-aware local trajectory re-planning immediately generates the recovery of the planned operation trajectory, which allows the robot to promptly re-execute the task operation. The recovery is computed as below

$$p_{ref}(t) = p^o_{ref}(t) + p_r(t), \tag{3}$$

where $p_r(t) = \bar{\gamma}(t)\bar{p}_c$ with $\bar{\gamma}(t)$ from 1 to 0 to generate smooth recover, and $\bar{p}_c$ being a constant vector containing the amount of correction calculated at the previous time instant. Compared with a repulsive force field-based collision avoidance methodology, our approach is free from local minima and undesired high generated robot end-effector accelerations [24]. Additionally, we do not employ a null-space-based collision avoidance, allowing us to apply our method also to non-redundant robot manipulators.

B. Human-Robot Seamless Close Interactions Control

The developed custom lightweight robotic arm presents n=6 actuated joints (degrees of freedom) and It is described with the following rigid-body dynamic model

$$M(q)\ddot{q} + C(q,\dot{q})\dot{q} + G(q) = \tau_c + J(q)^T w_{ext} \tag{4}$$

where $q, \dot{q}, \ddot{q} \in \mathbb{R}^n$ are joints position, velocity, and acceleration. $M(q) \in \mathbb{R}^{n\times n}$ is the inertia matrix, $C(q,\dot{q}) \in \mathbb{R}^{n\times n}$ is the Coriolis term, and $G(q) \in \mathbb{R}^n$ is the gravity vector. Then, $\tau \in \mathbb{R}^n$ is the joints torque command, $J(q) \in \mathbb{R}^{6\times n}$ is the Jacobian matrix, and $w_{ext} \in \mathbb{R}^6$ is the external wrench. The matrix $C(q,\dot{q})$ is given such that $\dot{M}(q) = C(q,\dot{q}) + C(q,\dot{q})^T$ holds and $\dot{M}(q) - 2C(q,\dot{q}) = 0$.

The motion control of the robotic arm is performed via PD plus feedforward torque control law with varying gains as

$$\tau_c = K_J(t)\bar{q} + D_J(t)\dot{\bar{q}} + \tau_{ff} \tag{5}$$

$\bar{q} = q_{ref} - q \in \mathbb{R}^n$ is the joints position error with $q_d \in \mathbb{R}^n$ the desired joints position. $\dot{\bar{q}} = \dot{q}_d - \dot{q} \in \mathbb{R}^n$ is the joints velocity error with $\dot{q}_{ref} \in \mathbb{R}^n$ the desired joints velocity ($\dot{q}_{ref} = 0$) [25]. $K_J(t) \in \mathbb{R}^{n\times n}$ and $D_J(t) \in \mathbb{R}^{n\times n}$ are the varying gain matrices related to the joint stiffness and damping, respectively. These matrices are assumed to be at least semi-positive definite. $\tau_{ff} \in \mathbb{R}^n$ is the feedforward torque computed as $\tau_{ff} = \tau_g + \tau_w$ where $\tau_g \in \mathbb{R}^n$ is the gravity torque vector, and $\tau_w = -J(q)^T w_{ext} \in \mathbb{R}^n$ is the torque related to an external wrench. The joint position references are generated via Inverse Kinematics $q_{ref} = f^{-1}(p_{ref})$.

Time-varying gains permit the realization of robot compliance as demanded in real-time. To deal with executing shared tasks, robot compliance is modulated according to the minimum level required to satisfy a demanded operation in such a way as to maintain the robot as compliant as possible to account for eventual contacts. In particular, the robot impedance is automatically adjusted by fulfilling operation requirements, described in terms of precision to satisfy and the wrench to apply. By applying a virtual linear spring to the robot end-effector, the desired Cartesian stiffness, chosen diagonal, $K^d_C = diag\{k^d_c\} \in \mathbb{R}^{6\times 6}$ is set based on the task operations requirements profiles as follows

$$K^d_C(t) = \frac{|w^d(t)|}{\Delta x^d(t)}, \tag{6}$$

IEEE Robotics and Automation Letters (RA-L) paper, presented at ICRA 2026, Vienna, Austria. Cite as RA-L paper.

where $w^d(t) = w_g(t) + w^o_{ref}(t) \in \mathbb{R}^6$ is the desired wrench at the robot end-effector, with $w_g \in \mathbb{R}^6$ the gravity wrench at the robot end-effector, and $\Delta x^d(t) = \Delta x^0_{ref}(t) \in R^6$. To derive the joint space stiffness from the Cartesian stiffness, the relationship between small displacements in task space and joint space is considered. Given an infinitesimal displacement in task space δx is related to a displacement in joint space δq as $\delta x = J\,\delta q$. In Cartesian space, displacement of force δf can be related in response to task displacement as $\delta f = K_c\,\delta x$. By substituting, we obtain $\delta f = K_c\,J\,\delta q$ and given $\delta\tau = J^\top \delta f$ we have $\delta\tau = J^\top K_c\,J\,\delta q$. Since joint stiffness K_j relates joint torque to joint displacement via $\delta\tau = K_j\,\delta q$, equating both expressions leads to $K_j = J^\top K_c\,J$. Therefore, the desired Cartesian stiffness computed based on the task operations requirements is realized via joint impedance as

$$K_J(t) = J(q)^T K^d_C(t) J(q),\;\; D_J(t) = 2\xi\sqrt{K_J(t)}. \quad (7)$$

As detailed in [26], the stiffness map owns two terms where the second $\frac{\partial J(q)^T}{\partial q} K^d_C(t)\Delta x_d(t) = 0$ when the stiffness is computed around the equilibrium or the robot is in an unloaded position. The joint damping is derived as in [27] where $\xi \in \mathbb{R}$ is the damping ratio. Selecting critical damping in the robot behavior enables smooth responses, eliminating overshoot and oscillations, crucial for safety in human-shared spaces. The time-varying gains of the control law (5) could produce issues for the system's stability. The following condition should hold

$$\dot{\bar{q}}^T D_J(t)\dot{\bar{q}} \geq \frac{1}{2}\bar{q}^T \dot{K}_J(t)\bar{q} \quad (8)$$

derived by applying the Direct Lyapunov method. $\dot{K}_J(t) \in \mathbb{R}^{n\times n}$ is the time derivative of the joints stiffness matrix. More details are available in [28], with the formal stability analysis and online verification.

V. EXPERIMENTS

The experiments carried out are: i) robot reaction showcase, ii) assisted assembly task, and iii) co-assembly task. i) shows the robot reactions generated by the proximity-aware local trajectory re-planning when a proximity sensor is triggered. Meanwhile, ii) and iii) demonstrate the system capabilities to enable human-robot seamless close interactions in shared-task execution. The experiments ii) and iii) differ in the shared workspace zones. In the experiment iii), the human and the robot work always on the same shared workspace: all the task operations occur in the same area, while in the experiment ii), the human and the robot work on task operations in different areas except in some areas where they are occasionally shared to exchange parts. Scenarios and setups are shown in Fig. 5. Experiments ii) and iii) were further conducted in comparison to the stop-and-wait approach to validate the proposed approach. In this case, the robot stops if the distance measurement is less than the defined safety distance, waiting to continue performing the task operations when the distance is recovered.

A. Experiments Description

Robot Reactions Showcase: In this experiment, the robot rests in a specific configuration, and a human goes closer to each sensor. When the set threshold for the distance is violated, the robot's reaction is triggered, and the robot starts to move away from the possible contact. All the sensors are used to demonstrate different robot reactions according to the different sensors triggered.

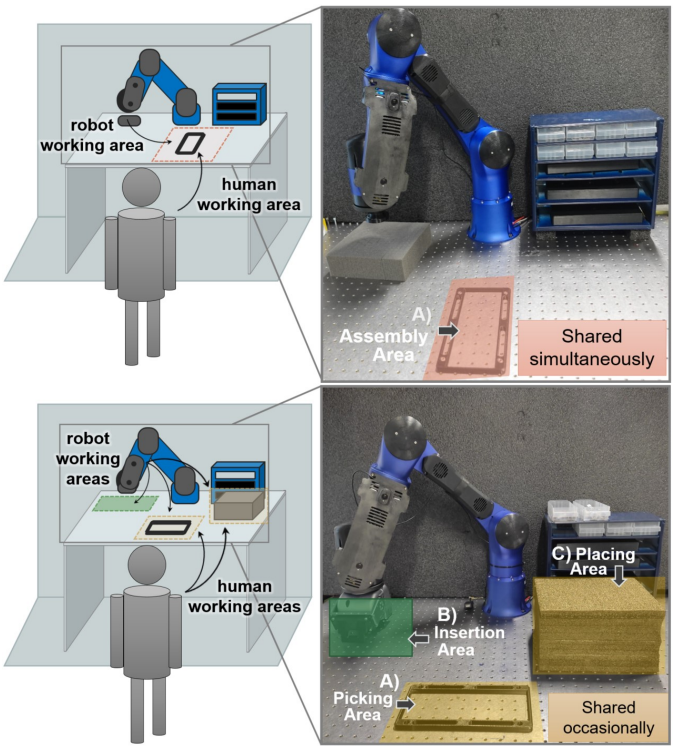

Fig. 5. *Experiments Setup*: (Top) human and robot work simultaneously in the same zone: red area, to accomplish a co-assembly task. (Bottom) Humans and robots work in different zones to accomplish an assisted-assembly task. The robot works independently in the green area while occasionally sharing some areas to exchange parts with the human in the yellow areas.

Assisted Assembly Task: In this task, the human and the robot share a common task. The task involves inserting steel pins in holes on dedicated boards and then screwing nut caps on top of them. The task of assisted assembly is synergetically executed, with the human working on the precision and dexterous part of the task: locating pins and screwing nut caps, while the robot performs the heavy part of the task: inserting the pins. The task execution occupies different zones in the working area. Considering the Fig. 5 bottom picture, the image shows the work area and the arrangement used during the experiment. The assembly pipeline is hereafter described. First, the robot goes to the area (A) to pick a board with the pins positioned on it by the human. Then, the robot moves into the area (B) to operate the insertion task (pressing the pins down) for each pin, and then it places the assembled object to the area (C) for the human to complete the task by screwing the nut caps on inserted pins. In this scenario, the human and the robot perform operations and share occasional workspace zones (A) and (C) to exchange parts. The assembly task is repeated for 3 boards inserting on each board 2 pins and screwing the nut caps on each pin.

Co-Assembly Task: In this task, the human and the robot again execute the same task operations, but simultaneously sharing a workspace during the entire execution, area (A) in the top picture of Fig. 5. Similarly to the *Assisted Assembly*

IEEE Robotics and Automation Letters (RA-L) paper, presented at ICRA 2026, Vienna, Austria. Cite as RA-L paper.

Task, the robot executes the heavy part of the task, and the human takes care of the precision and dexterous part of it. In this scenario, the robot does not have to grasp and bring the board object to another place, but it operates the insertion of the pins in the same zone as the human does. During the execution, the robot stays near the common area (A) waiting to insert pins. When pins are located, the robot proceeds to press them down. The pipeline is shown in Fig. 7. The assembly task is repeated for 3 boards inserting on them 3 pins and screwing the nut cap on each pin.

B. Experiments Settings

Robot Reactions Showcase: The robot rests in a predetermined configuration. No other settings were necessary to execute the experiment.

Assisted Assembly Task: To perform this task, a custom end-effector is used and in Fig. 7, the task pipeline is shown. The task is executed with different tracking errors according to the operation as follows.

- *Picking Board In Picking Area (Shared)*: To grasp the board in area (A), precise positioning of the end-effector is required. The approaching motion has a maximum tracking error of 0.02m along x and y required by the task, and 0.01m in the z-direction due to the presence of the table. To pick the board up, a maximum tracking error of 0.01m in all directions to precisely lift the board.
- *Placing Board In Inserting Area (Not Shared)*: Following this, the robot moves in a lateral position, area (B), with a maximum tracking error of 0.03m along x and y and 0.01m in z direction. Then, the board is released on the table without constraints. The tracking errors on x and y are relaxed to favor a lower stiffness while maintaining a higher tracking error on z due to the table.
- *Inserting Pins In Inserting Area (Not Shared)*: The pressing of the pins is performed with a tracking error of 0.01m in all directions to increase stiffness and exert the force.
- *Picking Board In Inserting Area (Not Shared)*: After pressing all the pins, the robot grasps the board with a maximum tracking error of 0.02m in x and y and 0.01m in z direction. Then, the board is lifted with a maximum tracking error of 0.03m in x and y and 0.02m in z. Here, the board is not constrained in a frame. Hence, the maximum tracking error is relaxed.
- *Placing Board In Placing Zone (Shared)*: The board with the inserted pins is transported to the desired area (C) with a tracking error of 0.05m on x and y and 0.02m on z, and leaving it down with a tracking error on z changed to 0.01m. Then, the robot moves to pick another board. In this shared area, we relax the error to ensure a lower stiffness behavior due to the human vicinity.

Co-Assembly Task: The robot has a dedicated end-effector, and the settings are:

- *Pressing Pins In Assembly Area (Shared)*: The robot moves on top of pins with a maximum tracking error of 0.02m in the z direction and 0.03m in the other two directions. Compared with the previous task, the tracking errors set is larger due to the large surface of the dedicated end-effector to press the pins. When the robot performs the pressing, the maximum tracking error is reduced to 0.01m along the z direction and to 0.02m along the other directions. Again, due to the end-effector's larger surface of pressing, x and y tracking errors are set larger compared with the previous case. Then, the robot moves aside at a distance equal to 0.10m, relaxing the maximum tracking error to 0.03m (z) and 0.05m (x,y), allowing the robot to be compliant in the close vicinity of the human.

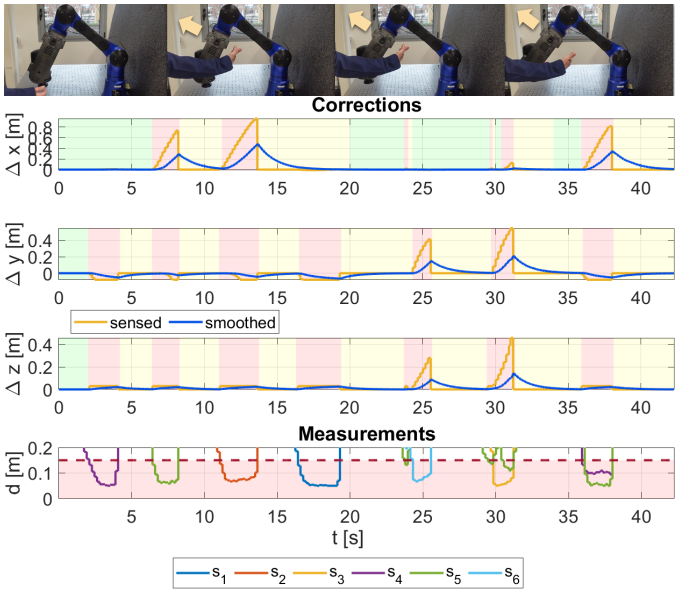

Fig. 6. *Robot Reactions Showcase*: The plots show i) corrections (top plots) calculated to move the robot away when the threshold is violated and recover over its initial configuration when the threshold is not violated anymore, and ii) sensor measurements (bottom plot) showing the violation of the threshold from the sensor's measurements.

The pressing (z direction) in both tasks had a force set equal to 10N. The tracking error was varied across task phases to make the robot stiff for precise actions and more compliant in shared spaces where humans might be present. The control runs on an embedded Linux PC using Xbot2 [29], [30] and CartesIO planner [31]. The maximum impedance was set 2000Nm/rad for stiffness and 50Nms/rad for damping. d_{safe} = 0.15m. The parameter settings were the same for the stop-and-wait approach except for the safety distance equal to 0.25m for ii) and 0.35m for iii).

C. Experiments Results

Robot Reactions Showcase: The robot rests in a specific configuration, and the proximity-aware local trajectory replanning computes the robot's end-effector trajectory modifications when the human violates the threshold as depicted in Fig. 6. In the corrections plots, the yellow line indicates the modification produced by the proximity sensor measurements. The blue line shows the resulting smoothed trajectory. In the Measurements plot, we show the distance measurements, highlighting the area of the safe distance threshold (red area). According to the sensors triggered, the trajectory modification is computed to avoid the collision (red area), followed by a recovery (yellow area). The green areas indicate that neither changes nor recovery are computed.

Assisted Assembly Task and Co-Assembly Task: To execute the overall task, the proposed framework uses task operations

IEEE Robotics and Automation Letters (RA-L) paper, presented at ICRA 2026, Vienna, Austria. Cite as RA-L paper.

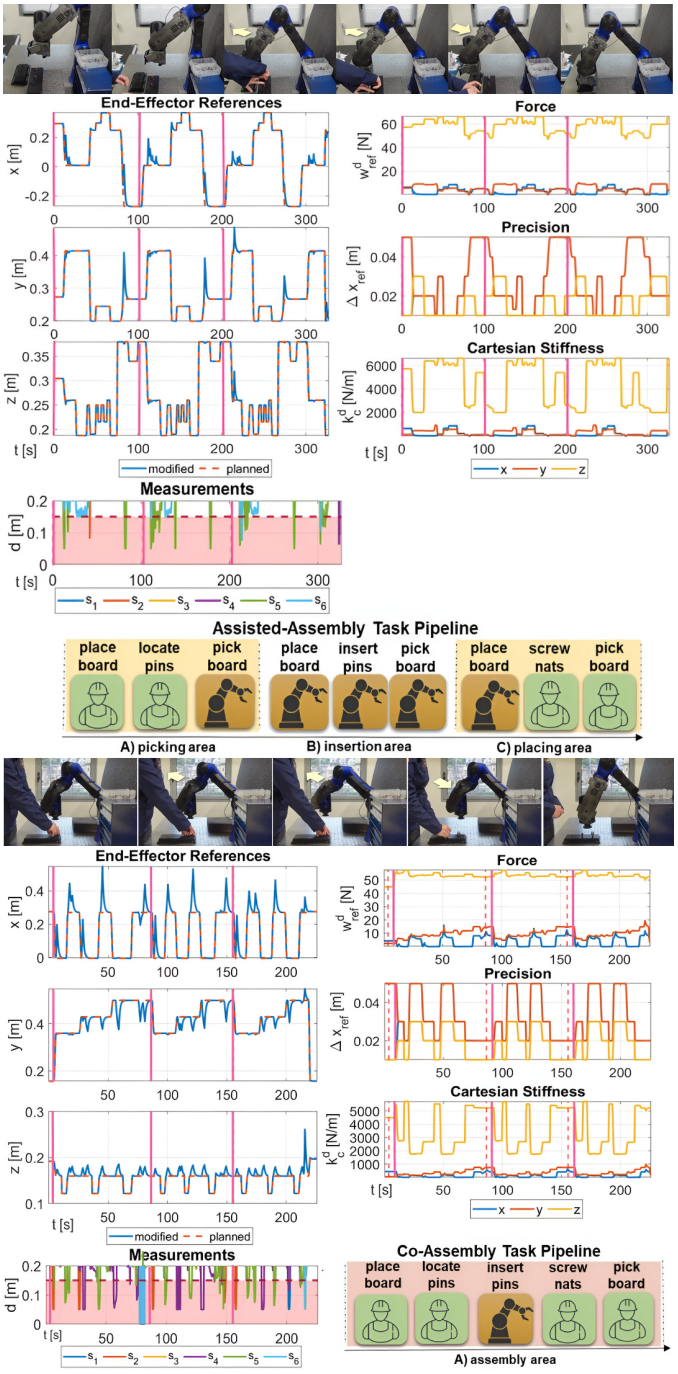

Fig. 7. *Assisted-Assembly Task (Top) and Co-Assembly Task Results (Bottom).* The plots show: i) end-effector references (left plots), ii) sensor measurements (left-bottom plot), and iii) generated Cartesian stiffness based on required task force and precision (right plots). The trajectory given by the global planner (orange line) and the refined trajectory provided by the proximity-aware local trajectory re-planning module (blue line) are shown. In the sensor measurements plot, the retrieved data are shown, particularly when they exceed the threshold for the distance (red dashed line). The Force and Precision plots display the related profiles generated by the global planner, while the Cartesian Stiffness plot is dictated by these Force and Precision profiles.

and task-specific requirements as input parameters, as detailed in Section V.B. The experimental results are shown in Fig. 7 for the assisted-assembly and co-assembly task execution. In both scenarios, the robot's reference trajectory (blue line, left plots) is dynamically computed by combining the operation trajectory (orange line) with real-time corrections from a proximity-aware local trajectory re-planning system. This re-planning mechanism is triggered when human proximity sensors detect a distance below a predefined safety threshold, indicated by entries falling within the red-shaded regions in the measurement plots (bottom left). These proximity-based corrections ensure safe and adaptive behavior during close human-robot interaction. The operation requirements (right plots) define the desired Cartesian stiffness, force, and precision profiles, which are critical for modulating joint stiffness and damping. This modulation enables compliant behavior essential for human-robot close interaction. The vertical pink lines denote the start of each board assembly cycle, repeated three times for both. Notably, even if the co-assembly scenario demonstrates more frequent and larger corrections in the reference trajectory, reflecting the robot's increased need for adaptation due to the human actively performing manipulation steps such as inserting pins and screwing nuts nearby the robot, this approach has a less time execution (Table III). This scenario also shows more variability in distance measurements across the sensors, highlighting the high dynamic nature of human-robot close interactions. Finally, the diagrams at the bottom of each figure illustrate the task pipeline for both scenarios. The assisted-assembly pipeline (bottom of the first figure) shows the robot executing most of the actions with human presence primarily in the picking and placing areas. In contrast, the co-assembly pipeline (bottom of the second figure) reflects a more collaborative setup where the human is directly involved in key assembly steps within a shared workspace, requiring the robot to operate with higher responsiveness and compliance.

TABLE III
TASK EXECUTION TIME (IN SECONDS)

Control Strategy	Scenario ii)	Scenario iii)
Stop-and-Wait	368	243
Reactive Motion	323	203

In the experiments using the stop-and-wait approach, the re-planned trajectory remained identical to the originally planned one, as no modifications were introduced during execution. Consequently, as illustrated in the plot of Fig. 7, the robot followed the same trajectory shown by the orange lines. However, the total execution time was longer, as also reflected in Table III. This increase in duration is primarily attributed to the robot's behavior of halting its motion entirely whenever the predefined safety distance was violated. Specifically, the robot stops moving if the distance measurement falls below the defined safety threshold, and waits until the distance is recovered before continuing task execution. This safety mechanism ensures human-robot separation but introduces delays during close interactions. Moreover, due to the absence of a reactive motion module, the robot could not dynamically adjust its trajectory in response to the human's position. As a result, it often remained stationary in close proximity to the human, leading to a reduced effective safety margin during execution. For consistency across all trials, the safety distance was set to 0.25 meters. While smaller thresholds could decrease execution time, they would increase the risk

IEEE Robotics and Automation Letters (RA-L) paper, presented at ICRA 2026, Vienna, Austria. Cite as RA-L paper.

of contact with the human operator. This behavior contrasts with experiments involving reactive motion, where the robot could continuously respond to the human's movement, actively maintain safe distances, and execute the task more efficiently. Time execution is shown in Table III are average over three executions. The key aspect of unlocking robots to work in human-shared environments while performing close interactions is the ability to monitor and evaluate the robot's close workspace constantly, jointly with the ability to generate and execute fast online robot trajectory adjustments able to efficiently negotiate undesired potential impacts. In a scenario where a camera-based system would be used, occlusions in the visual field could lead to false detections, prompting the robot to stop unnecessarily. Such interruptions may further increase the overall execution time. Therefore, these experiments indicate that close workspace monitoring realized via on-board proximity sensors with reactive motion is crucial for enabling human-robot seamless close interactions, removing unnecessary slowdowns or larger interruptions of operations due to i) camera occlusions, and/or ii) static reactive robot behavior, increasing the task performances and productivity.

Lastly, due to the custom prototype of the robot arm, some level of model uncertainty, as parameter estimation, could lead to the system's execution. However, the robot consistently followed the generated trajectories, indicating that the dynamic model was sufficiently accurate for implementing the proposed interaction control strategy and supporting the experimental evaluation. Potential negative effects of model inaccuracies could be mitigated by increasing the safety threshold. Methods as inertia scaling for safety may be more sensitive to modeling errors, as inaccuracies directly affect the scaled dynamics and could lead to unintended behavior. In this regard, our approach offers a more robust alternative under moderate model uncertainty. The experiments are available at https://youtu.be/XGVZGGSbcf8 and https://youtu.be/eirePd8hetE.

VI. CONCLUSIONS

We present a novel robotic system that permits human-robot seamless close interactions. We introduced a custom lightweight robotic arm equipped with on-board proximity sensing integrated into the forearm section and a complete control framework. The custom lightweight robotic arm is aimed at furnishing compliance and close workspace awareness. At the same time, the control framework provides the robot's reactions to negotiate potential contacts and proper impedance settings. Future works will concentrate on analyzing human behaviors in case of unavoidable contact with the expectation of increasing the safety of the overall system.

REFERENCES

[1] A. Ajoudani and et. al, "Progress and prospects of the human–robot collaboration," *Autonomous Robots*, vol. 42, pp. 957–975, 2018.

[2] O. Khatib, K. Yokoi, O. Brock, K. Chang, and A. Casal, "Robots in human environments: Basic autonomous capabilities," *The International Journal of Robotics Research*, vol. 18, no. 7, pp. 684–696, 1999.

[3] G. Hoffman, "Evaluating fluency in human-robot collaboration," *IEEE Transactions on Human-Machine Systems*, vol. 49, 2019.

[4] M. Eckhoff, R. J. Kirschner, E. Kern, S. Abdolshah, and S. Haddadin, "An mpc framework for planning safe & trustworthy robot motions," in *International Conf. on Robotics and Automation (ICRA)*. IEEE, 2022.

[5] M. Lagomarsino and et. al, "Maximising coefficiency of human-robot handovers through reinforcement learning," *IEEE Robotics and Automation Letters*, vol. 8, no. 8, pp. 4378–4385, 2023.

[6] V. Prasad, A. Kshirsagar, D. K. R. Stock-Homburg, J. Peters, and G. Chalvatzaki, "Moveint: Mixture of variational experts for learning human-robot interactions from demonstrations," *IEEE Robotics and Automation Letters*, 2024.

[7] L. Pérez and et al., "Symbiotic human–robot collaborative approach for increased productivity and enhanced safety in the aerospace manufacturing industry," *The International Journal of Advanced Manufacturing Technology*, vol. 106, no. 3, 2020.

[8] L. Scalera, A. Giusti, R. Vidoni, and A. Gasparetto, "Enhancing fluency and productivity in human-robot collaboration through online scaling of dynamic safety zones," *The International Journal of Advanced Manufacturing Technology*, vol. 121, no. 9-10, 2022.

[9] J. Vorndamme, A. Melone, R. Kirschner, L. Figueredo, and S. Haddadin, "Safe robot reflexes: A taxonomy-based decision and modulation framework," *IEEE Transactions on Robotics*, 2024.

[10] I. TC184/SC2, "Iso/ts 15066 robots and robotic devices – safety requirements for industrial robots," *Collaborative operation*, 2013.

[11] B. Lacevic, A. R. S. E. M. Newishy, A. M. Zanchettin, and P. Rocco, "Enhanced performance of human-robot collaboration using braking surfaces and trajectory scaling," in *IEEE/RSJ International Conference on Intelligent Robots and Systems (IROS)*. IEEE, 2023.

[12] R. Laha, W. Wu, R. Sun, N. Mansfeld, L. F. Figueredo, and S. Haddadin, "S*: On safe and time efficient robot motion planning," in *International Conference on Robotics and Automation (ICRA)*. IEEE, 2023.

[13] A. Pupa, M. Minelli, and C. Secchi, "A time-optimal energy planner for safe human-robot collaboration," in *IEEE International Conference on Robotics and Automation (ICRA)*. IEEE, 2024, pp. 17 373–17 379.

[14] A. Palleschi, M. Hamad, S. Abdolshah, M. Garabini, S. Haddadin, and L. Pallottino, "Fast and safe trajectory planning: Solving the cobot performance/safety trade-off in human-robot shared environments," *IEEE Robotics and Automation Letters*, vol. 6, no. 3, pp. 5445–5452, 2021.

[15] S. E. Navarro and et al., "Proximity perception in human-centered robotics: A survey on sensing systems and applications," *IEEE Transactions on Robotics*, vol. 38, no. 3, 2021.

[16] A. Hoffmann, A. Poeppel, A. Schierl, and W. Reif, "Environment-aware proximity detection with capacitive sensors for human-robot-interaction," in *2016 IEEE/RSJ International Conference on Intelligent Robots and Systems (IROS)*. IEEE, 2016, pp. 145–150.

[17] K.-E. M'Colo and et al., "Obstacle avoidance using a capacitive skin for safe human-robot interaction," in *IEEE/RSJ International Conference on Intelligent Robots and Systems (IROS)*. IEEE, 2019.

[18] S. J. Moon, J. Kim, H. Yim, Y. Kim, and H. R. Choi, "Real-time obstacle avoidance using dual-type proximity sensor for safe human-robot interaction," *IEEE Robotics and Automation Letters*, 2021.

[19] J. Thomas and F. Chaumette, "Positioning in congested space by combining vision-based and proximity-based control," *IEEE Robotics and Automation Letters*, 2024.

[20] Y. Ding and U. Thomas, "Collision avoidance with proximity servoing for redundant serial robot manipulators," in *IEEE International Conference on Robotics and Automation (ICRA)*, 2020.

[21] H. Alagi, S. Ergun, Y. Ding, T. P. Huck, U. Thomas, H. Zangl, and B. Hein, "Evaluation of on-robot capacitive proximity sensors with collision experiments for human-robot collaboration," in *International Conference on Intelligent Robots and Systems*. IEEE, 2022.

[22] M. Kamezaki, T. Wada, and S. Sugano, "Dynamic collaborative workspace based on human estimation for safe and productive human-robot collaboration," *IEEE Robotics Automation Letters*, 2024.

[23] "Terabee," 2023, https://www.terabee.com/ [Accessed: 2023].

[24] Y. Koren, J. Borenstein *et al.*, "Potential field methods and their inherent limitations for mobile robot navigation." in *Icra*, vol. 2, 1991.

[25] B. Siciliano and L. Villani, *Robot force control*. Springer Science & Business Media, 1999.

[26] A. Albu-Schaffer and et al., "Soft robotics: what cartesian stiffness can obtain with passively compliant, uncoupled joints?" in *IEEE/RSJ International Conference on Intelligent Robots and Systems*, 2004.

[27] L. M. Doornebosch, D. A. Abbink, and L. Peternel, "Analysis of coupling effect in human-commanded stiffness during bilateral tele-impedance," *IEEE Transactions on Robotics*, vol. 37, no. 4, 2021.

[28] L. Bertoni, L. Muratore, A. Laurenzi, and N. G. Tsagarakis, "Task driven online impedance modulation," in *2022 IEEE-RAS 21st International Conference on Humanoid Robots (Humanoids)*. IEEE, 2022.

[29] L. Muratore, A. Laurenzi, E. M. Hoffman, A. Rocchi, D. G. Caldwell, and N. G. Tsagarakis, "Xbotcore: A real-time cross-robot software platform," in *IEEE International Conf. on Robotic Computing*, 2017.

[30] A. Laurenzi and et al., "The xbot2 real-time middleware for robotics," *Robotics and Autonomous Systems*, vol. 163, 2023.

[31] A. Laurenzi, E. Hoffman, L. Muratore, and N. G. Tsagarakis, "Cartesi/o: A ros-based real-time capable cartesian control framework," in *International Conference on Robotics and Automation (ICRA)*. IEEE, 2019.